Appendix: Leveraging Distribution Alignment via Stein Path for Cross-Domain Cold-Start Recommendation

Weiming Liu, Jiajie Su, Chaochao Chen, and Xiaolin Zheng*
Zhejiang University, Hangzhou, China
{21831010,sujiajie,zjuccc,xlzheng}@zju.edu.cn

A Model

A.1 Procedure of Stein path distance

We first present the procedures of Stein path distance calculation in Algorithm 1. The calculation of Stein path distance mainly has three steps. First, adopting kernel density estimation [4, 3] with radial basis function kernel to estimate the source probability of $\boldsymbol{W}$ and $\boldsymbol{V}$ (line 1). Second, finding the Stein mirror point of the cold item auxiliary embeddings through SVGD (line 2-line 8). Third, calculating the Stein path distance (line 9).

A.2 Procedure of multiple-proxies

As mentioned in Section 2.3.3, the multiple-proxies algorithm is given by:

$$\min_{\boldsymbol{M},\boldsymbol{\psi}_i^T\mathbf{1}=1,\psi_{ij}\geq 0} \sum_{i=1}^{N}\sum_{j=1}^{H}\psi_{ij}||\boldsymbol{c}_i-\boldsymbol{m}_j||_2^2+\alpha\sum_{i=1}^{N}\sum_{j=1}^{H}\psi_{ij}\log\psi_{ij}, \tag{1}$$

where $\boldsymbol{c}_i$ denotes the i-th cold item auxiliary embeddings and $\boldsymbol{m}_j$ denotes the j-th corresponding proxy. We now provide the optimization details on the multiple-proxies algorithm. Alternatively updating $\boldsymbol{M}$ and $\boldsymbol{\Psi}$ can solve Equation (1) efficiently.

Update $\boldsymbol{\Psi}$. We first fix the variable $\boldsymbol{M}$ and update $\boldsymbol{\Psi}$. By using Lagrangian multiplier to minimize the objective function, we have:

$$\min_{\boldsymbol{\Psi}} L=\sum_{i=1}^{N}\sum_{j=1}^{H}\psi_{ij}||\boldsymbol{c}_i-\boldsymbol{m}_j||_2^2+\alpha\sum_{i=1}^{N}\sum_{j=1}^{H}\psi_{ij}\log\psi_{ij}+\varpi\sum_{i=1}^{N}\left(\sum_{j=1}^{H}\psi_{ij}-1\right). \tag{2}$$

Taking the differentiation of Equation (2) w.r.t. ψ_{ij} and setting it to 0, we obtain:

$$\frac{\partial L}{\partial\psi_{ij}}=||\boldsymbol{c}_i-\boldsymbol{m}_j||_2^2+\alpha(\log\psi_{ij}+1)+\varpi=\Omega_{ij}+\alpha(\log\psi_{ij}+1)+\varpi=0. \tag{3}$$

By solving and simplifying Equation (3), we have:

$$\psi_{ij}=\exp\left(-\frac{\alpha+\varpi+\Omega_{ij}}{\alpha}\right)=\exp\left(-\frac{\alpha+\varpi}{\alpha}\right)\exp\left(-\frac{\Omega_{ij}}{\alpha}\right). \tag{4}$$

Meanwhile, taking $\sum_{j=1}^{H}\psi_{ij}=1$ into Equation (4), we have:

$$\sum_{j=1}^{H}\exp\left(-\frac{\alpha+\varpi+\Omega_{ij}}{\alpha}\right)=\exp\left(-\frac{\alpha+\varpi}{\alpha}\right)\sum_{j=1}^{H}\exp\left(-\frac{\Omega_{ij}}{\alpha}\right)=1. \tag{5}$$

*Corresponding Author

35th Conference on Neural Information Processing Systems (NeurIPS 2021), Sydney, Australia.

Algorithm 1 The procedure scheme of Stein path distance $(\boldsymbol{X}^{\mathcal{S}}, \boldsymbol{X}^{\mathcal{T}})$

Input: T: training iteration; N: batchsize; D: latent dimension; σ: bandwidth in Gaussian Kernel function; $\boldsymbol{X}^{\mathcal{S}} \in \mathbb{R}^{N \times D}$: source samples; $\boldsymbol{X}^{\mathcal{T}} \in \mathbb{R}^{N \times D}$: target samples.
Procedure:

```
Estimate p_{X^S} through Kernel Density Estimation;
Initialize X^T_{i,0} = X^T_i;
for l = 1 to T do
    for i = 1 to N do
        For all j = 1, 2, ..., N, calculate k(X^T_{i,l-1}, X^T_{j,l-1}) = exp( - ||X^T_{i,l-1} - X^T_{j,l-1}||_2^2 / σ^2 );
        X^T_{i,l} = X^T_{i,l-1} + (1/N) Σ_{j=1}^{N} [ k(X^T_{i,l-1}, X^T_{j,l-1}) ∇_{X^T_{i,l-1}} log p_{X^S}(X^T_{i,l-1}) + ∇_{X^T_{i,l-1}} k(X^T_{i,l-1}, X^T_{j,l-1}) ];
    end for
end for
Calculate the Stein Path P_{T→S}(X^T) = (1/N) Σ_{i=1}^{N} ||X^T_{i,t} - X^T_{i,0}||_2^2;
Return: P_{T→S}(X^T);
```

That is,

$$\exp\left(-\frac{\alpha+\varpi}{\alpha}\right) = \frac{1}{\sum\limits_{j=1}^{H} \exp\left(-\frac{\Omega_{ij}}{\alpha}\right)}. \tag{6}$$

Thus, the final solution of ψ_{ij} is given by:

$$\psi_{ij} = \frac{\exp\left(-\frac{\Omega_{ij}}{\alpha}\right)}{\sum\limits_{k=1}^{H} \exp\left(-\frac{\Omega_{ik}}{\alpha}\right)}. \tag{7}$$

Update $\boldsymbol{M}$. After we have updated $\boldsymbol{\Psi}$, we fix it as a constant and update $\boldsymbol{M}$. Thus, Equation (1) becomes

$$\min_{\boldsymbol{M}} \sum_{i=1}^{N} \sum_{j=1}^{H} \psi_{ij} ||\boldsymbol{c}_i - \boldsymbol{m}_j||_2^2. \tag{8}$$

Taking the differentiation of Equation (8) w.r.t. $\boldsymbol{m}_j$ and setting it to 0, we can update $\boldsymbol{M}$ as:

$$\boldsymbol{m}_j = \frac{\sum\limits_{i=1}^{N} \psi_{ij} \boldsymbol{c}_i}{\sum\limits_{i=1}^{N} \psi_{ij}}. \tag{9}$$

We finally summarize the optimization of multiple-proxies in Algorithm 2.

Algorithm 2 The procedure scheme of Multiple-proxies

Input: t: training iteration; N: batch size; D: latent dimension; α: the hyper parameter between the main objective loss and regularization term; $\boldsymbol{C} \in \mathbb{R}^{N \times D}$: cold item auxiliary embedding;
Procedure:

```
Random initialize the proxies M.
for i = 1 to t do
    Updating Ψ through Equation.(7)
    Updating M through Equation.(9)
end for
Return: Ψ, M.
```

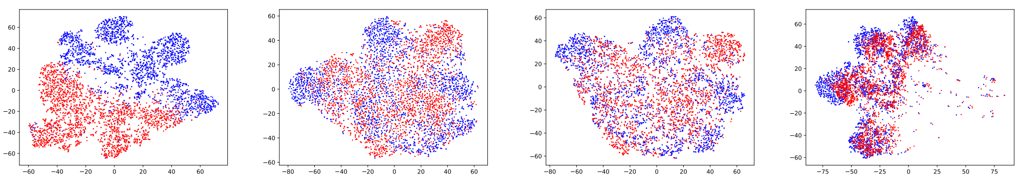

(a) Heater (b) ESAM (c) DARec (d) DisAlign-SP

Figure 1: The t-SNE visualization of **Amazon Movie→Amazon Music**. **Amazon Movie** is the warm domain with blue dots and **Amazon Music** is the cold-start domain with red dots.

A.3 Procedure of proxy Stein path loss

As we have presented in Section 2.3.3, the *proxy Stein path distance* is defined as:

$$\mathcal{P}^*_{\mathcal{T}\to\mathcal{S}}(\boldsymbol{M}) = \frac{1}{H}\sum_{i=0}^{H}||\boldsymbol{m}_{i,t} - \boldsymbol{m}_{i,0}||_2^2 = \frac{1}{H}\sum_{i=0}^{H}||\boldsymbol{m}_{i,t-1} + \epsilon\phi_{\mathcal{S}}(\boldsymbol{m}_{i,t-1}) - \boldsymbol{m}_{i,0}||_2^2, \tag{10}$$

where $\boldsymbol{m}_{i,t}$ denotes the i-th proxy $\boldsymbol{m}_i$ at the t-th iteration. Notably, in each batch, proxy Stein path *only* needs to move the number of proxy samples (H) in the target domain rather than the total number of samples (N). We now briefly demonstrate that the original target samples $\boldsymbol{C}$ can be updated by the typical proxies $\boldsymbol{M}$ through gradient descend. By taking the gradient of $\mathcal{P}^*_{C\to W}(\boldsymbol{M})$ w.r.t. $\boldsymbol{c}_{i,0}$, we have:

$$\begin{aligned}\frac{\partial\mathcal{P}^*_{C\to W}(\boldsymbol{M})}{\partial\boldsymbol{c}_{i,0}} &= \sum_{j=1}^{H}\frac{\partial\mathcal{P}^*_{C\to W}(\boldsymbol{M})}{\partial\boldsymbol{m}_{j,0}}\frac{\partial\boldsymbol{m}_{j,0}}{\partial\boldsymbol{c}_{i,0}} = \sum_{j=1}^{H}\left(-\frac{2}{H}\left(\boldsymbol{m}_{j,t} - \boldsymbol{m}_{j,0}\right)\right)\frac{\psi_{ij}}{\sum\limits_{i=1}^{N}\psi_{ij}} \\ &= \sum_{j=1}^{H}\left(-\frac{2}{H}\left(\boldsymbol{m}_{j,t} - \frac{\sum\limits_{i=1}^{N}\psi_{ij}\boldsymbol{c}_{i,0}}{\sum\limits_{i=1}^{N}\psi_{ij}}\right)\right)\frac{\psi_{ij}}{\sum\limits_{i=1}^{N}\psi_{ij}}.\end{aligned} \tag{11}$$

Obviously, $\boldsymbol{m}_{j,0}$ is the weighted sum of $\boldsymbol{C}$ according to Equation (9), therefore the cold item auxiliary embedding $\boldsymbol{C}$ can be updated through the typical proxies $\boldsymbol{M}$. We present the procedure of proxy Stein path loss in Algorithm 3.

Algorithm 3 The procedure scheme of proxy Stein path loss

Input: N: batchsize; D: latent dimension; $\boldsymbol{V} \in \mathbb{R}^{N\times D}$: warm item preference embedding; $\boldsymbol{W} \in \mathbb{R}^{N\times D}$: warm item auxiliary embedding; $\boldsymbol{C} \in \mathbb{R}^{N\times D}$: cold item auxiliary embedding;

Procedure:

1: Finding Multiple Proxies $\boldsymbol{M}$ on $\boldsymbol{C}$ through Algorithm 2.
2: Calculating the Stein Path distance $\mathcal{P}^*_{C\to W}(\boldsymbol{M})$ through Algorithm 1.
3: Calculating the Stein Path distance $\mathcal{P}^*_{C\to V}(\boldsymbol{M})$ through Algorithm 1.
4: **Return**: $L_{PSP} = \mathcal{P}^*_{C\to W}(\boldsymbol{M}) + \mathcal{P}^*_{C\to V}(\boldsymbol{M}) + ||\mathcal{P}^*_{C\to W}(\boldsymbol{M}) - \mathcal{P}^*_{C\to V}(\boldsymbol{M})||_2^2$.

B Experiment

B.1 Datasets

We conduct extensive experiments on two popularly used real-world datasets, i.e., *Douban* [6, 7] and *Amazon* [5, 2]. The details of Douban and Amazon datasets are shown in Table 1 and Table 2.

B.2 Visualization

To show feature transferability, we visualize the t-SNE embeddings [1] of the source item auxiliary embeddings ($\boldsymbol{W}$) and the target item auxiliary embeddings ($\boldsymbol{C}$). The results of Amazon

Table 1: Experimental datasets and tasks on Douban and Amazon datasets

Datasets	Items	Users	Interactions	Density
Douban Movie	34,893	2,712	1,278,401	1.35%
Douban Book	6,777	2,110	96,041	0.67%
Douban Music	5,567	1,672	69,709	0.75%
Amazon Movie (Movies and TV)	12,287	27,822	779,376	0.228%
Amazon Music (CDs and Vinyl)	7,710	11,053	296,188	0.348%

Table 2: Statistics on different CDCSR tasks

Source datasets	Target datasets	#Overlap users
Douban Book	Douban Movie	2,106
Douban Music	Douban Movie	1,666
Douban Music	Douban Book	1,562
Amazon Movie (Movies and TV)	Amazon Music (CDs and Vinyl)	2,782

Table 3: Ablation test on H

(Amazon) Book → Movie	$H=\sqrt{N}$	$H=\frac{1}{4}N$	$H=\frac{1}{3}N$	$H=\frac{1}{2}N$	$H=\frac{2}{3}N$	$H=\frac{3}{4}N$	$H=N$
HR	0.3447	0.3461	0.3471	0.3485	0.3480	0.3455	0.3428
Recall	0.2518	0.2524	0.2539	0.2542	0.2535	0.2522	0.2505
NDCG	0.1612	0.1624	0.1633	0.1644	0.1639	0.1625	0.1609

Movie→Amazon Music are shown in Figure 1. From it, we find that the conclusion is similar as Douban Movie→Douban Book, as we have reported in Section 3.2. That is: (1) **Heater** does not has the ability to bridge the gap across different domains, and thus the embeddings are separated in source and target domains, as shown in Figure 1(a); (2) **ESAM** and **DARec** have the tendency to draw the source and target embeddings closer, while they still have a certain distance, as shown in Figure 1(b) and Figure 1(c). This indicates that they can only align the marginal probability distribution; (3) `DisAlign`**-SP** in Figure 1(d) depicts that the embeddings trained through Stein path alignment achieve more closer gap between source and target domains.

B.3 Parameter Sensitivity

We also study the effect of hyper-parameters λ_{SP} and λ_{PSP} on our proposed `DisAlign`-SP and `DisAlign`-PSP. We vary λ_{SP} and λ_{PSP} in $\{0.1, 0.3, 0.5, 0.7, 1, 3, 10\}$ on two CDCSR tasks, i.e., **Douban Movie→Douban Book** and **Douban Book→Douban Movie**. Figure 2 shows the bell-shaped curve, indicating that choosing the proper hyper-parameters to balance the embedding distribution alignment loss and rating prediction loss can effectively improve the model performance. When $\lambda_{SP}, \lambda_{PSP} \to 0$, the embedding distribution module cannot play a part of role in the training process, causing the discrepancy between the source and target domains. Finding the proper trade-off between the rating prediction loss and embedding distribution alignment loss when $\lambda_{SP} = 0.5$ and $\lambda_{PSP} = 0.5$ can obtain the best performance on both datasets. Moreover, we even conduct the experiments on the $H = \{\sqrt{N}, \frac{N}{4}, \frac{N}{3}, \frac{N}{2}, \frac{2}{3}N, \frac{3}{4}N, N\}$ respectively on **Amazon Book → Amazon Movie**. The result has been shown in Table 3. In most cases, when the cold-item embedding space is clustered, the accuracy will gradually increase with the increase of H (e.g., from $H = \sqrt{H}$ to $H = \frac{N}{2}$). However, when H further approaches N, the accuracy will decrease since some outliers may cause side-effects. Meanwhile bigger H will cause longer time consumption. In our paper, to achieve a good balance between time complexity and prediction performance, we set $H = [\frac{N}{2}]$. In fact, one can set to a smaller value, e.g., $H = \sqrt{N}$, where the time complexity will decrease to $O(N^2)$. Naturally, this comes with some accuracy loss. However, the prediction accuracy of Proxy Stein path alignment still slightly outperforms Stein path alignment when the cold-item embedding space is clustered.

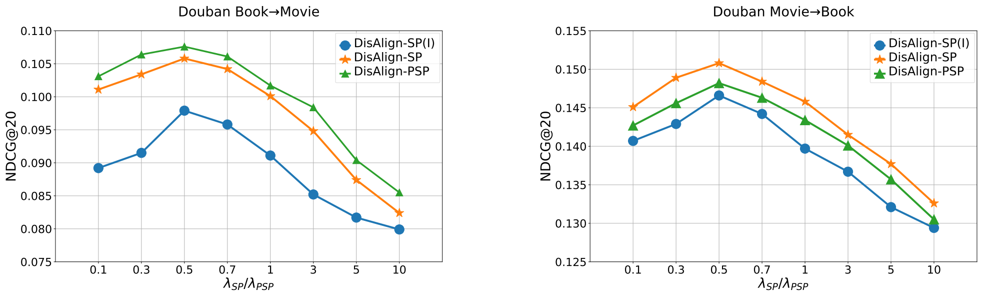

(a) (Douban) Book → Movie

(b) (Douban) Movie → Book

Figure 2: Effect of sensitivity λ_{SP} and λ_{PSP} on model performance.

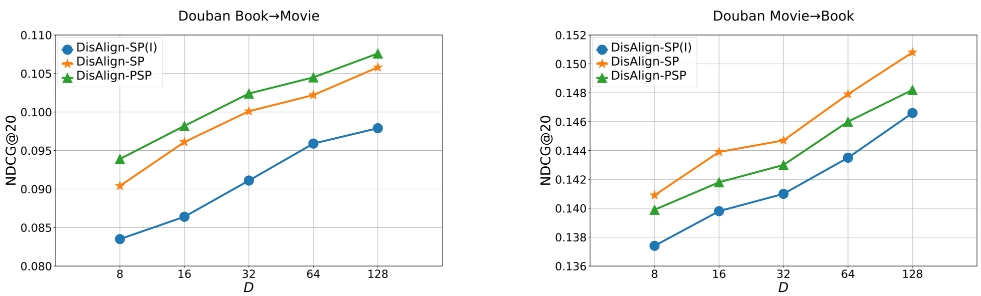

(a) Dimension on (Douban) Book → Movie

(b) Dimension on (Douban) Movie → Book

Figure 3: Effect of embedding dimension D on model performance.

B.4 Embedding Dimension

We finally analysis the effect of latent embedding dimension D on the performance of our proposed `DisAlign`-SP and `DisAlign`-PSP on two tasks, i.e., **Douban Movie→Douban Book** and **Douban Book→Douban Movie**. The results are shown in the Figure 3, where we range D in $\{8, 16, 32, 64, 128\}$. From it, we can see that, the recommendation accuracy of `DisAlign`-SP and `DisAlign`-PSP increase with D, which indicates that a larger embedding can provide a more accurate latent embeddings for both users or items.

References

[1] Van Der Maaten Laurens and Geoffrey Hinton. Visualizing data using t-sne. *Journal of Machine Learning Research*, 9(2605):2579–2605, 2008.

[2] Jianmo Ni, Jiacheng Li, and Julian McAuley. Justifying recommendations using distantly-labeled reviews and fine-grained aspects. In *EMNLP-IJCNLP*, pages 188–197, 2019.

[3] Travis A O'Brien, William D Collins, Sara A Rauscher, and Todd D Ringler. Reducing the computational cost of the ecf using a nufft: A fast and objective probability density estimation method. *Computational Statistics & Data Analysis*, 79:222–234, 2014.

[4] Travis A O'Brien, Karthik Kashinath, Nicholas R Cavanaugh, William D Collins, and John P O'Brien. A fast and objective multidimensional kernel density estimation method: fastkde. *Computational Statistics & Data Analysis*, 101:148–160, 2016.

[5] Cheng Zhao, Chenliang Li, Rong Xiao, Hongbo Deng, and Aixin Sun. Catn: Cross-domain recommendation for cold-start users via aspect transfer network. pages 229–238, 07 2020.

[6] Feng Zhu, Chaochao Chen, Yan Wang, Guanfeng Liu, and Xiaolin Zheng. Dtcdr: A framework for dual-target cross-domain recommendation. In *CIKM*, pages 1533–1542, 2019.

[7] Feng Zhu, Yan Wang, Chaochao Chen, Guanfeng Liu, and Xiaolin Zheng. A graphical and attentional framework for dual-target cross-domain recommendation. In *IJCAI*, pages 3001–3008, 2020.